

Opportunities for inclusive diffraction at EIC

Wojciech Słomiński^{1*}, Néstor Armesto², Paul R. Newman³, Anna M. Staśto⁴

1 Institute of Theoretical Physics, Jagiellonian University, Kraków, Poland

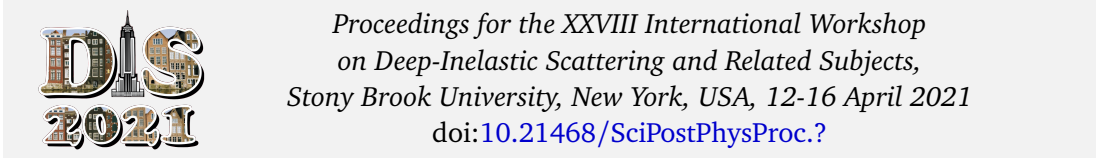
2 Instituto Galego de Física de Altas Enerxías IGFAE, Universidade de Santiago de Compostela, 15782 Santiago de Compostela, Galicia-Spain

3 School of Physics and Astronomy, University of Birmingham, UK

4 Department of Physics, Penn State University, University Park, PA 16802, USA

* wojtek.slominski@uj.edu.pl

July 6, 2022



Abstract

The possibilities for inclusive diffraction in the Electron Ion Collider, EIC, in the US, are analyzed. We find that thanks to the excellent forward proton tagging, the EIC will be able to access a wider kinematical range of longitudinal momentum fraction and momentum transfer of the leading proton than at HERA. This opens up the possibility to measure sub-leading diffractive exchanges. The extended t -range would allow the precise extraction of 4-dimensional reduced cross section in diffraction. In addition, the varying beam energy setups at the EIC would allow for precise measurements of the longitudinal diffractive structure function.

1 Introduction

Diffraction in DIS, as observed at HERA, consists a large ($\sim 10\%$) fraction of all inclusive events in DIS [1, 2], see the review [3] and refs. therein. In these events the proton stays intact or dissociates into a state with the proton quantum numbers. The experimental signature of such events is a final proton registered in a far forward detector, and/or the presence of a large rapidity gap (LRG) — the former case corresponds to a coherent diffraction where the proton does not get diffractively excited. The hadronic structure of the t -channel exchange in these events has been measured at HERA, and parametrized by means of diffractive parton densities.

In this presentation we discuss possibilities of measuring inclusive diffraction at EIC [4]. We describe the physical picture behind the performed studies and briefly present the obtained results. For some more plots the reader is advised to consult the slides of the [talk](#).

2 Cross section, structure functions and DPDFS

In Fig. 1 we show a diagram depicting a neutral current diffractive deep inelastic event in the one-photon exchange approximation. Charged currents could also be considered but in this presentation we limit ourselves to neutral currents.

The incoming electron or positron, with four momentum k , scatters off the proton, with incoming momentum p , and the interaction proceeds through the exchange of a virtual photon with four-momentum q .

The distinguishing feature of the diffractive event $ep \rightarrow eXY$ is the presence of the diffractive system of mass M_X and the forward final proton (or its low-mass excitation) Y with four momentum $p' = (E', \vec{p}_\perp, x_L p_z)$.

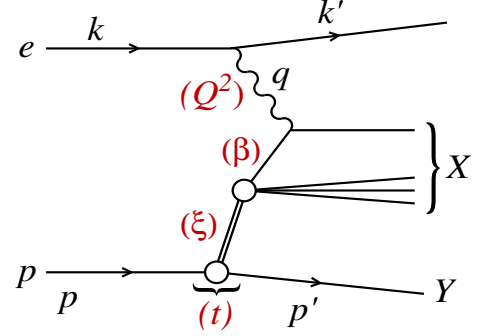


Figure 1: A diagram of a diffractive NC event in DIS together with the corresponding variables.

In addition to the standard DIS variables, diffractive events are also characterized by

$$t = (p - p')^2 = -\frac{p_\perp^2 + (1 - x_L)^2 m_p^2}{x_L}, \quad \xi = \frac{Q^2 + M_X^2 - t}{Q^2 + W^2}, \quad \beta = \frac{Q^2}{Q^2 + M_X^2 - t}. \quad (1)$$

Here t is the squared four-momentum transfer in the proton vertex, ξ (alternatively denoted by x_p) can be interpreted as the momentum fraction of the ‘diffractive exchange’ with respect to the hadron, and β is the momentum fraction of the parton with respect to the diffractive exchange. The two momentum fractions combine to give Bjorken- x , $x = \beta \xi$.

The physical picture suggested by Fig. 1 is that the initial proton splits into a final state Y of momentum $p' \simeq (1 - \xi)p$ and the object which is responsible for the diffractive exchange of momentum ξp . The latter, in turn, undergoes a DIS-like process to produce the final state X . The study presented in the following concerns coherent diffraction (i.e. the non-dissociative case), where the final state Y is a proton. Experimentally, this requires tagging of the final proton, which was performed at HERA using Roman pot insertions to the forward beam-pipe. At EIC we will have much better forward tagging capabilities which is discussed in Sec. 6. Note that, as compared to HERA, the EIC has rather limited possibilities of the LRG detection, mainly because of a lower energy range, but also because of the current detector design.

Diffractive cross sections in the neutral current case can be expressed in terms of the reduced cross sections

$$\frac{d^4\sigma^D}{d\xi d\beta dQ^2 dt} = \frac{2\pi\alpha_{\text{em}}^2}{\beta Q^4} Y_+ \sigma_r^{\text{D}(4)}(\beta, \xi, Q^2, t), \quad (2)$$

where $Y_+ = 1 + (1 - y)^2$. The reduced cross sections are, in turn, expressed by two diffractive structure functions F_2^D and F_L^D . In the one-photon approximation, the relation reads

$$\sigma_r^{\text{D}(4)} = F_2^{\text{D}(4)}(\beta, \xi, Q^2, t) - \frac{y^2}{Y_+} F_L^{\text{D}(4)}(\beta, \xi, Q^2, t). \quad (3)$$

The 3-dimensional reduced cross sections, $\sigma_r^{D(3)}(\beta, \xi, Q^2)$, as well as the structure functions, $F_{2,L}^{D(3)}$, fulfil analogous relations upon integration over t .

Within the standard perturbative QCD approach based on colinear factorization [5] the structure functions read

$$F_{2/L}^{D(4)}(\beta, \xi, Q^2, t) = \sum_i \int_{\beta}^1 \frac{dz}{z} C_{2/L,i} \left(\frac{\beta}{z} \right) f_i^{D(4)}(z, \xi, Q^2, t), \quad (4)$$

where the sum goes over all parton flavors (gluon, quarks), and the coefficient functions $C_{2/L,i}$ are the same as in inclusive DIS. The diffractive parton densities (DPDF) f_i^D (that fulfill DGLAP evolution) are modeled as a sum of two exchange contributions, \mathcal{P} and \mathcal{R} :

$$f_i^{D(4)}(z, \xi, Q^2, t) = f_i^P(\xi, t) f_i^{\mathcal{P}}(z, Q^2) + f_i^R(\xi, t) f_i^{\mathcal{R}}(z, Q^2). \quad (5)$$

For both of these terms proton vertex factorization is assumed, meaning that the diffractive exchanges can be interpreted as colorless objects called a ‘Pomeron’ or a ‘Reggeon’ with parton distributions $f_i^{\mathcal{P}, \mathcal{R}}(\beta, Q^2)$. The ‘Reggeon’ term is the only subleading exchange in this model, which was enough to parametrize the HERA data. The flux factors $f_{\mathcal{P}, \mathcal{R}}^P(\xi, t)$ are parametrized using the form motivated by the Regge theory,

$$f_{\mathcal{P}, \mathcal{R}}^P(\xi, t) = A_{\mathcal{P}, \mathcal{R}} \frac{e^{B_{\mathcal{P}, \mathcal{R}} t}}{\xi^{2\alpha_{\mathcal{P}, \mathcal{R}}(t)-1}}. \quad (6)$$

3 Data simulation

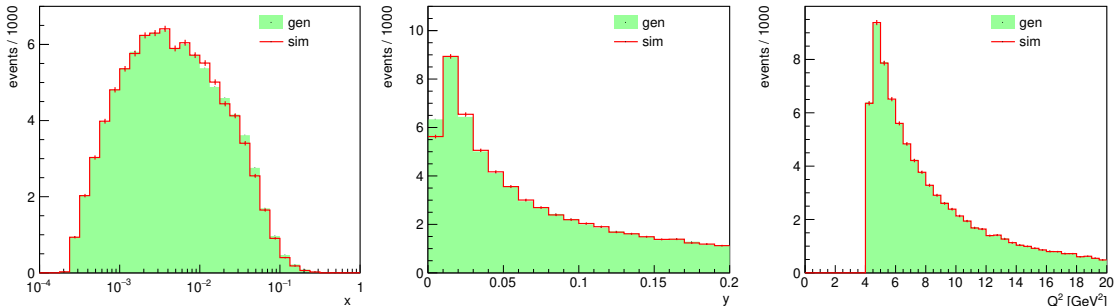


Figure 2: EIC detector acceptance for the standard DIS variables for $E_e = 18$ GeV and $E_p = 275$ GeV. Green area — Rapgap generated data; red histograms — reconstructed from the detector smeared data.

The process of generating pseudo-data is based on three ingredients: extrapolation, binning selection and systematic error assumption.

The calculation of extrapolated cross section for the ep diffractive DIS at EIC follows the model described in Sec. 2. The reduced cross sections for selected values of (β, ξ, Q^2, t) are obtained by performing the NLO DGLAP evolution starting from the ZEUS-SJ parametrization [6] of the diffractive PDFs. For a detailed description see Ref. [7].

For the $\sigma_r^{D(3)}$ simulations we assume a logarithmic binning with 4 bins per decade in each of β, Q^2, ξ . In order to assure that the EIC detector can provide high quality data for the selected

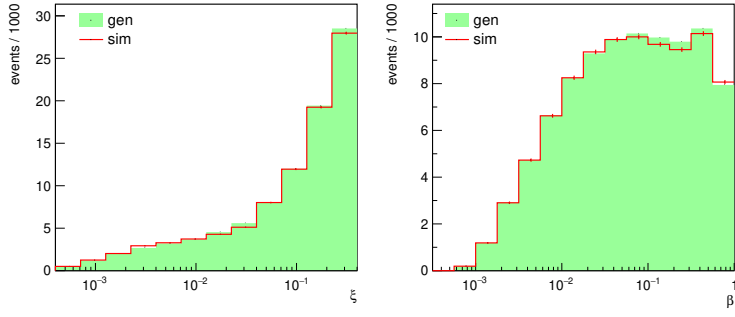


Figure 3: Same as Fig. 2 but for diffractive variables ξ and β .

binning we perform a detailed Monte-Carlo study where the data generated by the Rapgap MC generator ([8], see also <https://rapgap.hepforge.org/>) are passed through the detector simulation (using the EICsmear code [4]). Several kinematic reconstruction methods are considered leading finally to an optimized method consisting in taking an average from several of them weighted by their resolution. Within this optimized method a very good acceptance is achieved, as shown in Figs. 2 and 3.

Once the bins are fixed we calculate the cross sections and add random Gaussian smearing according to the estimated δ_{stat} and δ_{sys} added in quadrature. δ_{stat} is calculated from the cross section value and the assumed integrated luminosity of 2 or 10 fb^{-1} ; δ_{sys} is taken in the 1–5% range. Except for very large Q^2 (above 500 GeV^2), the errors of simulated data are dominated by δ_{sys} .

4 Diffractive PDFs from fits to pseudo-data

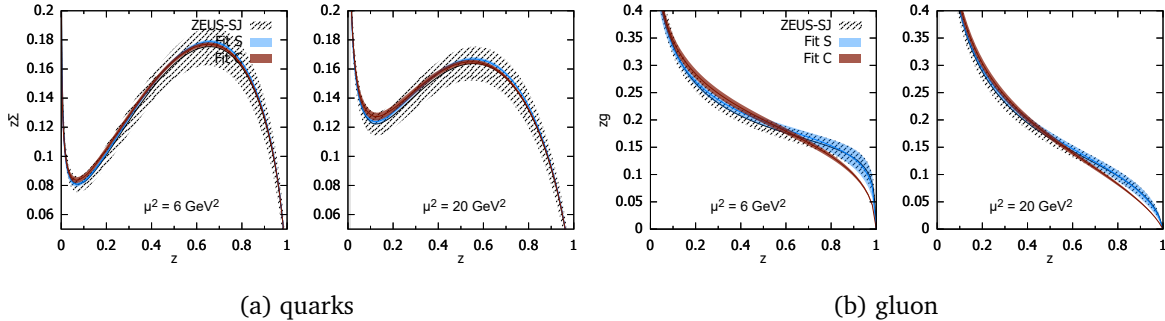


Figure 4: DPDFs from fits to the pseudo-data for $E_e = 18 \text{ GeV}$ and $E_p = 275 \text{ GeV}$.

The diffractive parton distribution functions were extracted from the fits to pseudo-data following the procedure explained in Ref. [7]. As compared to HERA we observe much smaller uncertainty for the quark DPDFs, at least at high values of the longitudinal momentum fraction z ($z \geq \beta$). The extraction of gluon DPDFs from the inclusive data only requires access to very low z and thus we get no improvement with respect to HERA.

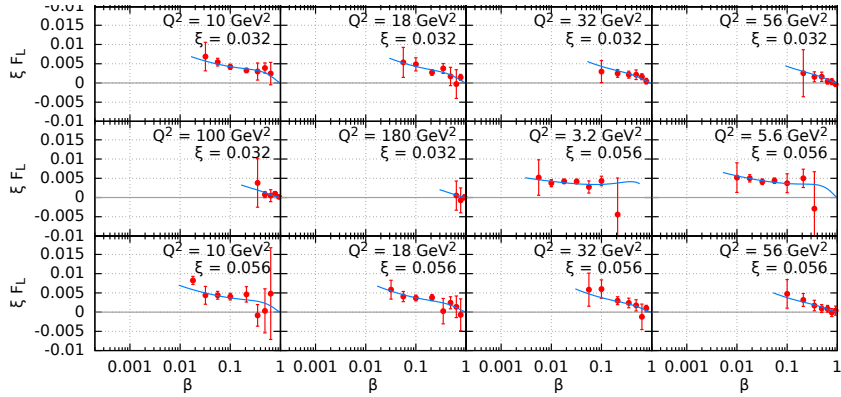


Figure 5: $F_L^{D(3)}$ from fits to pseudo-data simulated at 17 center-of-mass energies for $\delta_{\text{sys}} = 2\%$ and integrated luminosity of 10 fb^{-1} — a small subsample.

5 Longitudinal structure function

At fixed (β, ξ, Q^2) the reduced cross section $\sigma_r^{D(3)}$ depends on the center-of-mass energy squared, s , via the inelasticity $y = Q^2/(s\beta\xi)$,

$$\sigma_r^{D(3)} = F_2^{D(3)}(\beta, \xi, Q^2) - Y_L F_L^{D(3)}(\beta, \xi, Q^2), \quad (7)$$

where $Y_L = y^2/Y_+$.

This, rather weak, dependence comes from the non-zero longitudinal structure function $F_L^{D(3)}$ and is practically measurable at high y only. Precise measurements at several center-of-mass energies can provide data on $F_{2,L}^{D(3)}$ by fitting (7) as a function of Y_L .

To explore the possibility of such a measurement we considered three electron energies $E_e = 5, 10, 18 \text{ GeV}$ and 6 proton energies $E_p = 41, 100, 120, 165, 180, 275 \text{ GeV}$, resulting in 17 different center-of-mass energies. For the assumed binning we obtained 469 (β, ξ, Q^2) bins, each containing at least four $\sigma_r^{D(3)}$ data points. After fitting we got $F_L^{D(3)}$ vs. β plots in 76 (ξ, Q^2) bins. Some examples are shown in Fig. 5.

6 4-dimensional diffractive cross section

The EIC detector provides an excellent tagging of the final proton in a wide range of t and x_L . In Fig. 6 we show the kinematic range covered at three proton energies. In each plot the range covered by HERA is marked with a gray rectangle, and we see that EIC opens a new area for measurements of the leading proton.

In order to simulate data for the reduced cross section $\sigma_r^{D(4)}$ we have first performed the study of acceptance for the assumed binning of the variables related to the proton tagging, t, x_L, p_\perp , as described in Sec. 3. We have confirmed a very good agreement of the reconstructed vs. simulated data.

The results of simulations for $\delta_{\text{sys}} = 5\%$ and integrated luminosity of 10 fb^{-1} are shown in Fig. 7. It can be seen that the dependence of $\sigma_r^{D(4)}$ on both t and ξ can be measured with a very good precision. In particular, the double slope structure of the ξ dependence allows for a clear separation of the leading and subleading exchange contributions according to (5).

7 Conclusion

We have studied the capabilities of the EIC to measure diffraction in the inclusive DIS. We observe an excellent final proton tagging and a very good acceptance and resolution for the diffractive DIS variables.

Using simulated data for $\sigma_r^{D(3)}$ and $\sigma_r^{D(4)}$ we point out the possibilities of a precise extraction of the quark DPDFs, a measurement of $F_L^{D(3)}$ in a wide kinematic range and a precise determination of the subleading exchange contribution from the t -dependence studies.

Acknowledgements

We thank Hannes Jung for useful discussions. NA acknowledges financial support by Xunta de Galicia (Centro singular de investigación de Galicia accreditation 2019-2022); the "María de Maeztu" Units of Excellence program MDM2016-0692 and the Spanish Research State Agency under project FPA2017-83814-P; European Union ERDF; the European Research Council under project ERC-2018-ADG-835105 YoctoLHC; MSCA RISE 823947 "Heavy ion collisions: collectivity

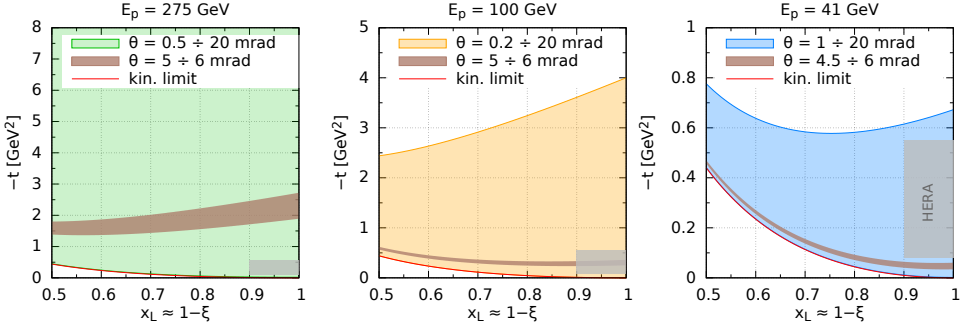


Figure 6: Final proton tagging. x_L, t range of the proton tagged by the EIC detector for three proton energies, 275 GeV, 100 GeV and 41 GeV. The brown strip marks a small (~ 1 mrad) region not covered by the current detector design.

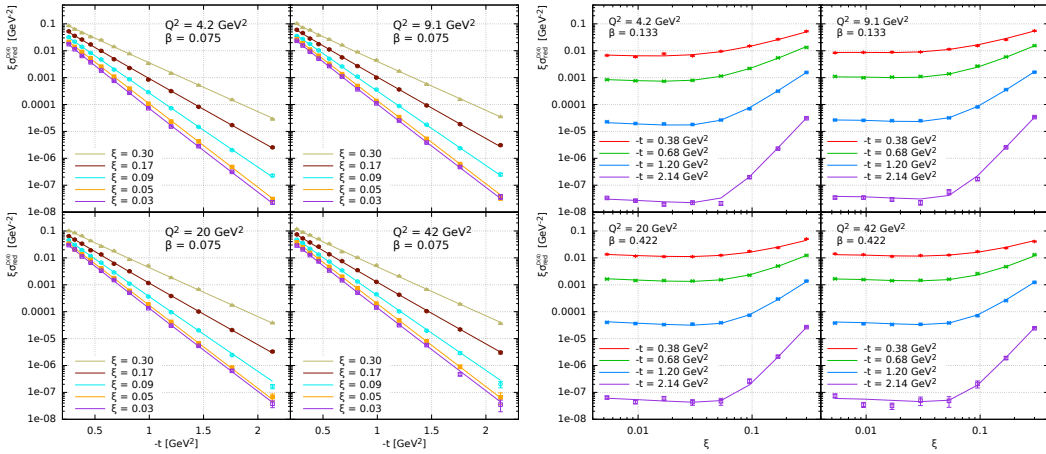


Figure 7: $\sigma_r^{D(4)}$ dependence on t and ξ in selected (Q^2, β) bins.

and precision in saturation physics" (HIEIC); and European Union's Horizon 2020 research and innovation programme under grant agreement No. 824093. AMS is supported by the U.S. Department of Energy grant No. DE-SC-0002145 and in part by National Science Centre in Poland, grant 2019/33/B/ST2/02588.

References

- [1] C. Adloff *et al.*, *Inclusive measurement of diffractive deep inelastic ep scattering*, Z. Phys. **C76**, 613 (1997), doi:[10.1007/s002880050584](https://doi.org/10.1007/s002880050584), hep-ex/[9708016](https://arxiv.org/abs/hep-ex/9708016).
- [2] J. Breitweg *et al.*, *Measurement of the diffractive structure function $F2(D(4))$ at HERA*, Eur. Phys. J. **C1**, 81 (1998), doi:[10.1007/s100520050063](https://doi.org/10.1007/s100520050063), hep-ex/[9709021](https://arxiv.org/abs/hep-ex/9709021).
- [3] P. Newman and M. Wing, *The Hadronic Final State at HERA*, Rev. Mod. Phys. **86**(3), 1037 (2014), doi:[10.1103/RevModPhys.86.1037](https://doi.org/10.1103/RevModPhys.86.1037), [1308.3368](https://arxiv.org/abs/1308.3368).
- [4] R. Abdul Khalek *et al.*, *Science Requirements and Detector Concepts for the Electron-Ion Collider: EIC Yellow Report* (2021), [2103.05419](https://arxiv.org/abs/2103.05419).
- [5] J. C. Collins, *Proof of factorization for diffractive hard scattering*, Phys. Rev. **D57**, 3051 (1998), doi:[10.1103/PhysRevD.61.019902](https://doi.org/10.1103/PhysRevD.61.019902), [10.1103/PhysRevD.57.3051](https://doi.org/10.1103/PhysRevD.57.3051), [Erratum: Phys. Rev.D61,019902(2000)], hep-ph/[9709499](https://arxiv.org/abs/hep-ph/9709499).
- [6] S. Chekanov *et al.*, *A QCD analysis of ZEUS diffractive data*, Nucl.Phys. **B831**, 1 (2010), doi:[10.1016/j.nuclphysb.2010.01.014](https://doi.org/10.1016/j.nuclphysb.2010.01.014), [0911.4119](https://arxiv.org/abs/0911.4119).
- [7] N. Armesto, P. R. Newman, W. Słomiński and A. M. Staśto, *Inclusive diffraction in future electron-proton and electron-ion colliders*, Phys. Rev. D **100**(7), 074022 (2019), doi:[10.1103/PhysRevD.100.074022](https://doi.org/10.1103/PhysRevD.100.074022), [1901.09076](https://arxiv.org/abs/1901.09076).
- [8] H. Jung, *Hard diffractive scattering in high-energy e p collisions and the Monte Carlo generator RAPGAP*, Comput. Phys. Commun. **86**, 147 (1995), doi:[10.1016/0010-4655\(94\)00150-Z](https://doi.org/10.1016/0010-4655(94)00150-Z).